

EGb761 Ameliorates Neuronal Apoptosis and Promotes Angiogenesis in Experimental Intracerebral Hemorrhage via RSK1/GSK3 β Pathway

Chao Pan¹ · Na Liu¹ · Ping Zhang¹ · Qian Wu¹ · Hong Deng¹ · Feng Xu¹ · Lifei Lian¹ · Qiming Liang¹ · Yang Hu¹ · Suiqiang Zhu¹ · Zhouping Tang¹ 

Received: 16 October 2016 / Accepted: 28 December 2016
© Springer Science+Business Media New York 2017

Abstract Neuronal apoptosis after intracerebral hemorrhage (ICH) plays an essential role in neurological deterioration. Preclinical studies have shown that EGb761, an extract of *Ginkgo biloba*, is neuroprotective in some other neurological diseases with apoptosis. This study was conducted to investigate the potential neuroprotective effect of EGb761 on neuronal apoptosis in experimental ICH. A model of ICH was induced in C57BL/6 mice by injecting collagenase. EGb761 was administered for 21 days and neurologic behaviors were assessed at 1, 3, 7, 14, and 21 days after ICH. RNAi-mediated knockdown of p90 ribosomal S6 kinase 1 (RSK1) was used to further investigate the role of RSK1 in EGb761-induced neuroprotective effects. Neuronal death was determined by TUNEL staining. The image datasets of neurovascular networks were acquired via micro-optical sectioning tomography (MOST). The glycogen synthase kinase-3 β (GSK3 β) activity

was assayed using commercial kit. Primary cultured cortical neurons were exposed to ferrous iron and treated with EGb761. Apoptotic neurons were counted by flow cytometry. RSK1, GSK3 β , phosphorylated-GSK3 β (pGSK3 β), Bcl2, Bax, cleaved-caspase3 (CC3), and VEGF were measured by Western blot. The pGSK3 β was also detected by immunofluorescence staining. We found that mice in EGb761 group performed better on rotarod test. Reduced TUNEL-positive neurons and richer microvascular networks were observed in mice treated with EGb761. EGb761 attenuates neuronal apoptosis induced by ferrous iron counted by flow cytometry in vitro. Decreased GSK3 β activity was observed in EGb761-treated mice compared with mice with ICH. EGb761 increased the expression of pGSK3 β (Ser9), RSK1 and the Bcl2/Bax ratio, and VEGF and decreased CC3 expression. In conclusion, EGb761 reduces neuronal apoptosis and

Electronic supplementary material The online version of this article (doi:10.1007/s12035-016-0363-8) contains supplementary material, which is available to authorized users.

✉ Suiqiang Zhu
zhusuiqiang@163.com

✉ Zhouping Tang
ddjtzp@163.com

Chao Pan
punctualpc@163.com

Na Liu
liuna_2003abc@163.com

Ping Zhang
ppkitty0609@163.com

Qian Wu
841646577@163.com

Hong Deng
15271814330@163.com

Feng Xu
xufengyang9@163.com

Lifei Lian
lianlifei@gmail.com

Qiming Liang
liang28917@163.com

Yang Hu
huyang081991@126.com

¹ Department of Neurology, Tongji Hospital, Tongji Medical College, Huazhong University of Science and Technology, Wuhan 430030, People's Republic of China

promotes angiogenesis in experimental intracerebral hemorrhage via RSK1/GSK3 β pathway.

Keywords Intracerebral hemorrhage · Neuroprotection · Glycogen synthase kinase-3 beta · Apoptosis · Angiogenesis

Introduction

Intracerebral hemorrhage (ICH) accounts for more than 15% of all types of stroke and is a global public health concern [1, 2] with an annual incidence of 10–30 per 100,000 population, accounting for 2 million (10–15%) of about 15 million strokes worldwide each year [1, 3–5]. It is characterized by sudden attack and prolonged treatment. Its pathogenesis and pathophysiological mechanism are poorly understood. ICH lacks effective therapies, resulting in high mortality and poor functional outcomes [1, 6, 7].

Accidental cerebrovascular rupture is followed by brain injury. Primary brain injuries are mostly mechanical tissue damage. Rapid hematoma in the brain parenchyma leads to brain tissue compression or disruption, elevated intracranial pressure, and blood–brain barrier destruction. Subsequently, a complex series of inflammatory, oxidative stress, and apoptotic pathways are triggered by degradation products of hematoma such as thrombin, hemoglobin, heme, and ferrous iron. Neurons in the perihematoma area undergo apoptosis and neurological functions deteriorate [7–9].

Originally identified as a regulator of glucose metabolism, glycogen synthase kinase 3 beta (GSK3 β) has also been found to be involved in a diversity of physiological and pathogenesis processes including inflammation, cell cycle progression, and cell apoptosis [10, 11]. Activated GSK3 β was involved in conducting neuronal apoptosis in a series of neurodegeneration and cerebrovascular diseases [12–15]. The activity of GSK3 β can be increased by phosphorylation at tyrosine-216 in GSK3 β and decreased by phosphorylation at serine-9 located in the N-terminal domain through multiple regulatory mechanisms such as the AKT/GSK3 β , PKC/GSK3 β /NF- κ B, and Wnt/GSK3 β signaling pathways [12, 15]. Among those regulatory pathways, p90 ribosomal S6 kinase 1 or ribosomal S6 kinase 1 (RSK1), one of the isoforms of a serine-threonine protein kinase RSK (90-kDa ribosomal S6 kinase) family, was reported to inhibit GSK3 β activity through phosphorylation of GSK3 β at serine-9 thereby attenuating the apoptosis mediated by GSK3 β [16–18].

EGb761, containing ginkgo flavonoid glycosides (24%); terpene trilactones (5.4–6.6%); ginkgolides A, B, and C (2.8–3.4%); and bilobalide (2.6–3.2%), is the standardized extract of *Ginkgo biloba* leaves [19]. Basic and clinical studies suggest that EGb761 alleviates the damage due to various neurological disorders, such as Alzheimer's disease (AD), subarachnoid hemorrhage (SAH), and Parkinson's disease

(PD) [20–23]. EGb761 administration markedly decreased neuronal necrosis and cell apoptosis and improved functional performance in rats during the acute phase after spinal cord contusion injury [24]. Also, EGb761 was found to inhibit hippocampal neuron apoptosis in rats with ischemic/reperfusion injuries [25]. In the rat primary cultures of cortical neurons, EGb761 was found to prevent zinc-induced activation of p38 MAPK and glycogen synthase kinase 3 beta (GSK3 β) and inhibited the neuropathology of AD [26]. EGb761 also promotes VEGF expression in Wistar rats after SAH [27]. Accordingly, we postulated that targeted inhibition of GSK3 β activity with EGb761 may improve neurological outcome after ICH by relieving neuronal apoptosis and enhancing angiogenesis, via downregulation of GSK3 β activity and promotion of VEGF expression.

In this study, we investigated the role of EGb761 in amelioration of behavioral outcomes, inhibition of neuronal apoptosis, and angiogenesis in experimental ICH mice model and primary cultured neurons. The RSK1/GSK3 β pathway was hypothesized and tested as the possible mechanism of EGb761 effects.

Methods

Animal Grouping, Drug Administration, and RSK1 shRNA Injection

The experimental protocols were approved by the Animal Center of Huazhong University of Science and Technology (Wuhan, China). Male C57BL/6 mice (age 8–10 weeks; weight, 20–25 g; Beijing HFK Bioscience Co. Ltd. China) were housed under a controlled environment at a temperature of 20 to 23 °C, and 12-h light–dark cycle, with free access to food and water.

Mice were randomly divided into four groups: (1) sham group ($n = 20$), (2) ICH model group ($n = 40$), (3) vehicle group ($n = 60$, intraperitoneally injected with saline for 21 days after ICH), and (4) EGb761 group ($n = 60$, intraperitoneally injected with 100 mg/kg EGb761) [28]. The initiation of EGb761 treatment was started from day 1 after ICH to day 21.

To further evaluate the relation between RSK1 and GSK3 β , RNA interference (RNAi)-mediated knockdown of RSK1 was used. Lentiviral vectors (GV298)-RSK1-small hairpin RNA (shRNA) (52364–21) were generated and purchased from Genechem Co., Ltd., Shanghai, China. RSK1-shRNA was designed based on the siRNA sequence which efficiently suppressed RSK1 expression in the mouse heart cell line (HL-1) [29]. The prepared RSK1-shRNA sequence was 5-GGA CCA AGA UGG AGA GAG ACA UCC T-3 (sense) and 5-AGG AUG UCU CUC UCC AUC UUG GUC CGA-3 (antisense). We stereotactically injected the RSK1 shRNA ($n = 4$) and control shRNA ($n = 4$) (Shanghai

Genechem Co., Ltd.) into the lateral ventricle (coordinates 0.5 mm posterior; 0.7 mm lateral to the bregma; and a depth of 2.5 mm from the surface of the brain before modeling. Then, the mice were sacrificed and the brains were collected at day 7.

Mouse ICH Models

ICH model was induced in mice by injecting collagenase type VII (Sigma, St. Louis, MO, USA) as previously described [30]. Briefly, male C57BL/6 mice were anesthetized with an intraperitoneal injection of 10% chloral hydrate (10 mL/kg) and held in a stereotaxic frame in prone position (Model 500, Kopf Instruments, Tujunga, CA, Beijing, China). A burr hole was drilled on the skull. Using a microinfusion pump, 0.0375 U collagenase in 0.5 μ L saline was stereotactically injected slowly into the right basal ganglia (coordinates 0.2 mm anterior, 3.5 mm ventral, and 2.5 mm lateral to the bregma). After injection, the needle was left for an additional 15 min and withdrawn at a rate of 1 mm/min. The surgical wound was sutured.

Behavioral Tests

Behavioral function was double-blindly assessed at days 1, 3, 7, 14, and 21 with modified neurological severity scores (mNSS) and rotarod (Ugo Basile, Comerio, Italy) test [31]. Mice with consciousness disorders or severe paralysis were excluded from the rotarod test. Before initiation of the rotarod test, mice were trained on rotarod at a set rotational speed (15 rpm) for 15 min, followed by three trials with an accelerating rotational speed from 4 to 40 rpm within 5 min to obtain baseline latency for 3 days prior to surgical operation. Each mouse was then tested for three times. The average retention time on rotarod was recorded.

TUNEL Staining

Mice were transcardially perfused with phosphate-buffered saline and 4% paraformaldehyde. The brains were collected and postfixed for 24 h in 4% PFA and then were dehydrated using 30% sucrose. Brain specimens at day 7 were embedded in paraffin, and neuronal apoptosis was determined with TUNEL staining using in situ Cell Death Detection Kit (Roche) as indicated in the manufacturer's instructions. Sections were observed using a Zeiss LSM 710 laser-scanning confocal fluorescence microscope (Zeiss, Jena, Germany). Images were analyzed with Zen software (Zeiss, Jena, Germany) and Image-Pro Plus 6.0 software (Media Cybernetics, CA, USA).

Reconstruction of 3D Neurovascular Networks

Mouse brain samples at day 21 were prepared as previously reported [32, 33]. Nissl-stained mouse brains were imaged by MOST to obtain 10,000 slices of coronal dataset, respectively. Coronal slices (10,000) were produced from original images by a series of preprocessing steps, which include trimming of redundant images, alignment of neighboring image strips, and illumination calibration of whole slice. Based on coronal datasets, sagittal datasets were obtained by reslicing using ImageJ 1.50b (National Institutes of Health, USA). A series of images was generated by minimum intensity projection of every 50 coronal slices to obtain neuronal soma and vessel network information. Three-dimensional ranges of normal brain structures and lesions were confirmed using ImageJ. Three-dimensional data blocks including lesions and normal structures were extracted, respectively, from continuous preprocessed coronal images using customized Matlab R2014a (MathWorks, USA) and processed via background normalization using low pass filter. Normalized data blocks include neural somas in the background and vessels in the foreground. Data blocks were obtained through grayscale inversion with soma in the foreground. Data blocks including soma were used to detect the location of soma using improved NucleusEditor software in Farsight Project. Data blocks including vessels were used to trace vessel centerline using the AutoSkeleton module in Amira 5.4.3 (FEI, USA). Data blocks including lesions were used to determine the three-dimensional outline of lesion structures employing the Segmentation module in Amira software. The contralateral normal structure was obtained symmetrically. Based on the determination of soma and vessel centerline, the final segmentation of soma and vessel inside the three-dimensional outline was extracted. Soma densities were determined according to the location and three-dimensional outline volumes. Based on vessel tracing results, the TREES toolbox v1.15 (open source) was used to perform quantitative analysis.

GSK3 β Activity Assay

Activity of GSK3 β of brain tissues at day 7 was measured using the GENMED GSK3 β Activity Assay Kit (GENMED Scientifics INC., Arlington, MA, USA) following the product instructions.

Cell Culture, Ferrous Iron Exposure, and Treatment

We developed primary cortical neuron cultures following a previously described method [34, 35]. Briefly, cells were dissociated from cortical tissues of neonatal C57 BL/6 mouse with 0.125% trypsin (Invitrogen) for 15 min at 37 °C. Cells were resuspended in a DMEM medium (Gibco, Carlsbad, CA, USA) containing 10% fetal bovine

serum (Gibco, Carlsbad, CA, USA) and seeded on six-well poly-L-lysine-coated culture plates. The medium was replaced after 6 h, and 50% of the medium was refreshed every 3 days with Neurobasal Medium (Gibco, Grand Island, NY) supplemented with 2% B27, 1% penicillin-streptomycin, and 1% L-glutamine (all from Sigma-Aldrich). To simulate hemorrhagic injuries *in vitro*, we added ferrous iron (FeSO₄) into the medium for 24 h at day 10 of growth [36, 37]. The cells were grouped into different categories for 24 h and then harvested for apoptosis assay and Western blot: (a) normal control, (b) FeSO₄ (5 μM), (c) EGb761 (20 μg/L), (d) FeSO₄ (5 μM) plus EGb761 (20 μg/L), and (e) FeSO₄ (5 μM) plus EGb761 (100 μg/L).

Cell Apoptosis Assay

Cell apoptosis assay was determined by flow cytometry using (labeling) the Annexin V-FITC Apoptosis Detection kit (Sigma-Aldrich) as reported previously [36]. Briefly, after being harvested from plates, the cells were washed with phosphate-buffered saline and resuspended into a concentration of 1×10^6 . Cell suspension was subsequently stained with Annexin V-FITC and propidium iodide (PI) for 15 min at room temperature in the dark. Apoptotic neurons (annexin V-FITC+/PI-) were detected on a flow cytometer (Becton Dickinson, USA) and analyzed with Flowjo software (version 7.6).

Western Blot

Cerebral tissues surrounding the hematoma were isolated and the cultured cells were harvested for Western blot. Brain tissues and cells were lysed and homogenized with RIPA lysis buffer supplemented with PMSF. Nuclear and cytoplasmic proteins were extracted using NE-PER nuclear and cytoplasmic extraction reagents (Thermo Scientific). Western blot was conducted as previously described [38, 39]. Membranes were incubated overnight with the following primary antibodies: anti-pGSK3β (Ser9) (1:1000, Cell Signaling, USA), anti-pGSK3β (Tyr216) (1:1000, Santa Cruz, USA), anti-GSK3β (1:1000, Cell signaling, USA), anti-RSK1 (1:1000, Santa Cruz, USA); anti-Bcl2 (1:1000, Abcam, UK), anti-Bax (1:1000, Abcam, UK), anti-CC3 (1:1000, Cell Signaling, USA); anti-VEGF (1:500, Abcam, UK), anti-DM1A (1:1000, Sigma, USA), anti-Histone3 (1:1000, Cell Signaling, USA), and anti-GAPDH (1:1000, Abcam, UK), and secondary antibodies. Bands were visualized with Odyssey Infrared Imaging System (Licor Biosciences, Lincoln, NE, USA), and the intensity of each lane was analyzed using ImageJ 1.50b (National Institutes of Health, USA).

Immunofluorescence Staining

After the procedure of fixation and dehydration described above, brain specimens were embedded in paraffin for double immunofluorescence. Brain slices were incubated overnight at 4 °C with primary antibodies including anti-NeuN (1:1000, Abcam, UK) and anti-pGSK3β (Ser9) (1:100, Cell Signaling, USA). Sections were observed using a Zeiss LSM 710 laser-scanning confocal fluorescence microscope (Zeiss, Jena, Germany). Images were analyzed with Zen software (Zeiss, Jena, Germany).

Statistical Analysis

Statistical analyses were performed with SPSS software, version 17.0. Data were expressed as mean ± S.E.M. For data to meet the normal distribution and equal variance (F test), Student's *t* test and one-way ANOVA followed by Turkey post hoc test were applied. Otherwise, Mann-Whitney U tests were employed (neurological severity scores and rotarod tests). The difference was considered significant at $p < 0.05$.

Results

EGb761 Alleviates Behavioral Deficits and Neuronal Death and in Mice After ICH

We used the modified neurological severity score (mNSS) and rotarod tests to determine the recovery of neurological function. We found no significant differences in mNSS between animals in the ICH, vehicle, and EGb761 groups (Fig. 1A). In the rotarod tests, mice treated with EGb761 performed better than did the other mice, remaining significantly longer on the rotarod stick from day 14 until day 21 (Fig. 1B). These data indicated that EGb761 treatment for 14 days resulted in faster recovery than in mice in the vehicle group up to 21 days.

TUNEL-positive neuronal cells were counted on day 7 posthemorrhage (Fig. 1C). The number of TUNEL-positive neurons was greater in the ICH group than in the sham group, which was significantly decreased by EGb761 treatment.

EGb761 Improves Angiogenesis via Increased VEGF Expression

The three-dimensional density of the microvessels was compared by reconstruction of all the vessels in the fields of lesion and contralateral areas. As shown in Fig. 2C, the microvessel density was higher in the lesions of EGb761-treated mice, when compared with the vehicle group. Therefore, we used Western blot to determine the VEGF levels and found that EGb761 administration enhanced the VEGF protein

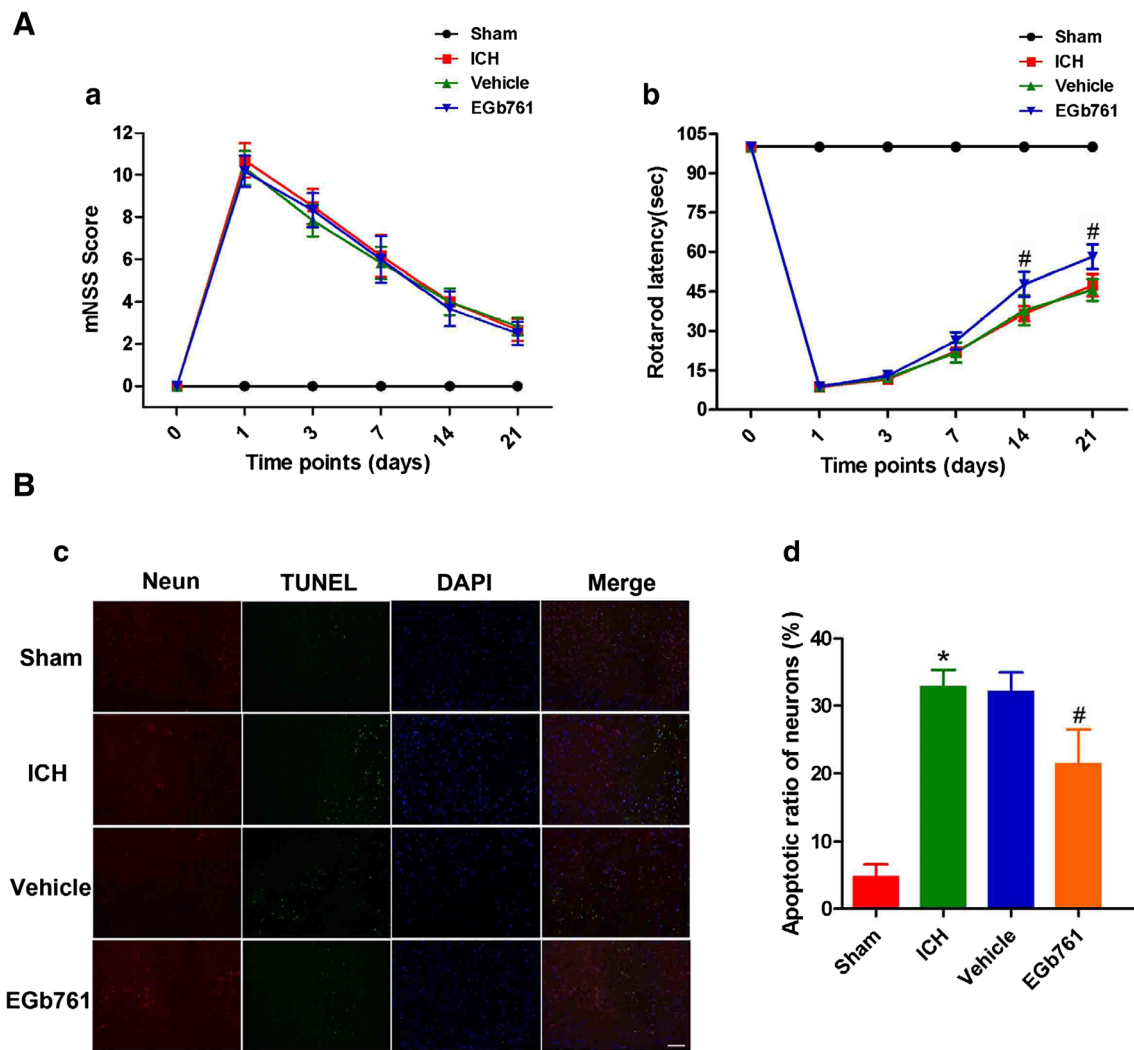


Fig. 1 Neurological functions were assessed by modified neurological severity score (mNSS) and rotarod tests. TUNEL staining was used to measure the neuronal death at day 7. **A** No obvious differences in mNSS score were observed between vehicle group and EGb761 group ($n = 10$, each group). **B** Rotarod test analysis revealed that mice in the EGb761 group performed better than those in the vehicle-treated groups from day

14 to day 21 ($n = 10$, each group; # $p < 0.05$ vs. vehicle group). **c** TUNEL-positive neurons were counted and the increase of TUNEL positive neurons was significantly attenuated in EGb761 group ($n = 6$, each group; * $p < 0.05$, as compared with the sham group; # $p < 0.05$, as compared with the vehicle group. Scale bar = 400 μm)

expression (Fig. 2D), which may explain the richer microvessel density caused by EGb761.

EGb761 Ameliorates Ferrous Iron-Induced Neuronal Apoptosis in Primary Cultured Neurons

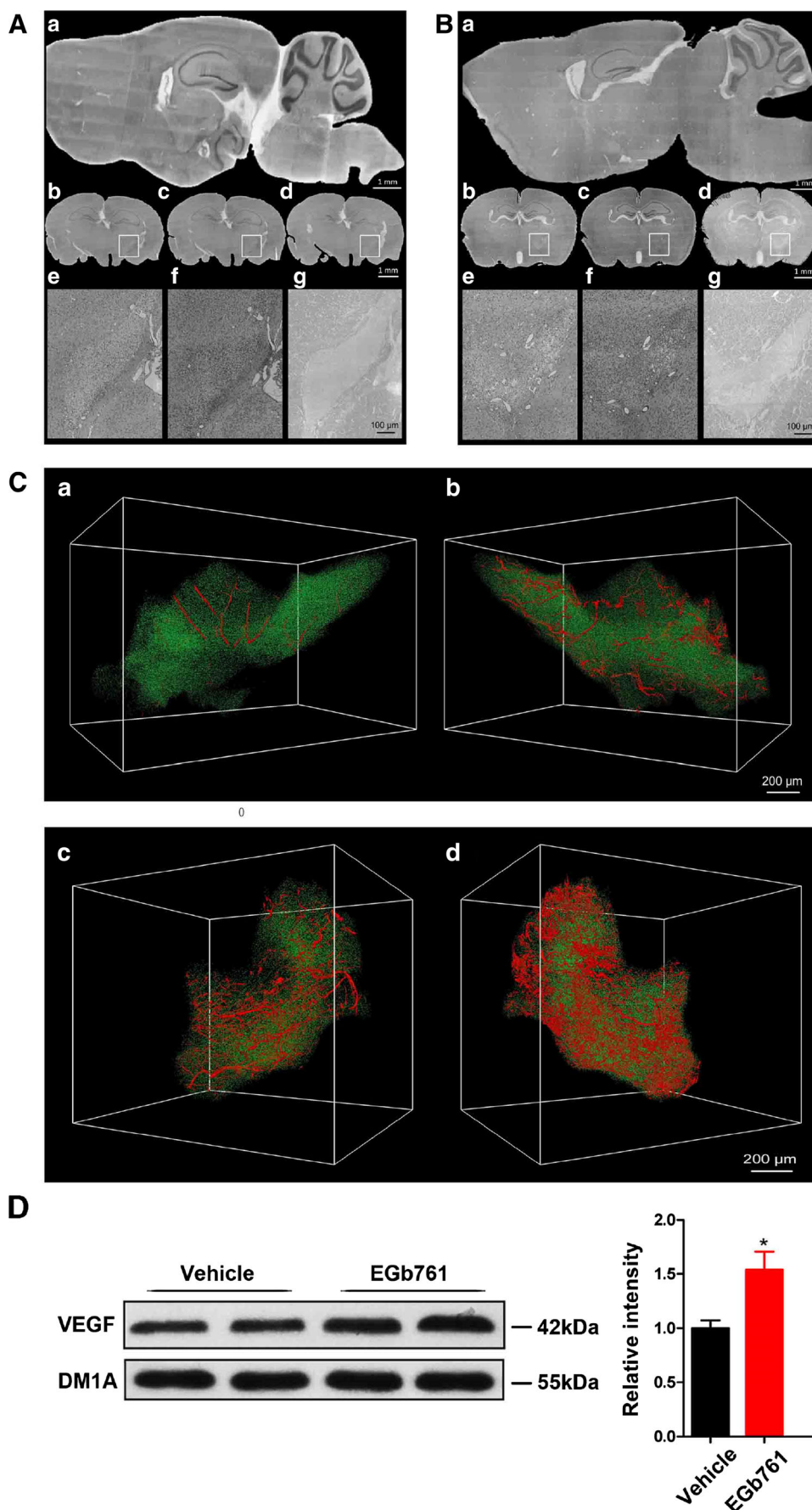
Flow cytometry was used to quantify ferrous iron-induced neuronal apoptosis. As shown in Fig. 3, few apoptotic cells (annexin V-FITC+/PI-) were detected in the normal and EGb761 groups. After exposure to ferrous iron, apoptosis increased markedly. Treatment with 20 and 100 $\mu\text{g/L}$ EGb761 prior to ferrous iron exposure dramatically decreased the apoptotic rates respectively.

EGb761 Suppresses GSK3 β Activity via RSK1/GSK3 β Pathway

The activity of GSK3 β after ICH is still unknown. Here, we measured GSK3 β activity in mouse brain tissues on day 7 after ICH. The data showed that the activity of GSK3 β was dramatically increased (almost fourfold) compared with that of the sham group in 7 days and decreased under EGb761 treatment (Fig. 4A).

As the activity of GSK3 β was modulated by phosphorylation at Ser9 (inactive) and Tyr216 (active) [38], we determined these two phosphorylation sites using Western blot. As shown in Fig. 4B, the pGSK3 β (Ser9) level was higher in the ICH group compared with the levels in the sham group, which may

Fig. 2 The sagittal views of the brain slices containing hematoma (thickness 1 μm) are demonstrated here (**A a**, **B a**). **A b** and **B b** show the raw images of cell and vessel structures in coronal view. The locations of hematomas in the brains were in almost the same position (caudate nucleus). **A c** and **B c** show the cytoarchitectures of the coronal sections; **A d** and **B d** show the vessel structures of the coronal sections (thickness 1 μm). In **A** and **B**, **e**, **f**, and **g** are the magnified images of **b**, **c**, and **d**, respectively. 3D reconstructions of neurons and vessels were acquired via matching coronal sections. **C** Representative 3D reconstruction video screenshot of a mouse brain in the vehicle and EGb761 groups, respectively. The regions in the video covered the lesion area (**b**, **d**), and the contralateral area (**a**, **c**). From the screenshot images, we can find that the microvessel density was higher in the lesions of the EGb761-treated mice, when compared with the vehicle group. To investigate the underlying mechanism, VEGF was detected with Western blot. In **D**, we can see a higher level of VEGF expressed in the EGb761-treated mice than in the vehicle mice ($n = 4$, each group; $*p < 0.05$, as compared with vehicle group), which may probably explain the phenomenon observed via MOST. *Green spots* shown in the screenshots represent cells stained by Nissl dye. Due to cell apoptosis and blood-brain barrier disruption, cell debris and degradation products could be non-specifically stained by Nissl dye, which may explain the increase in cell number counted in 3D images of the lesion side (**C b** 394,940/ mm^3 , **d** 318,239/ mm^3) compared with the unaffected normal side (**C a** 168,209/ mm^3 , **c** 165,873/ mm^3)



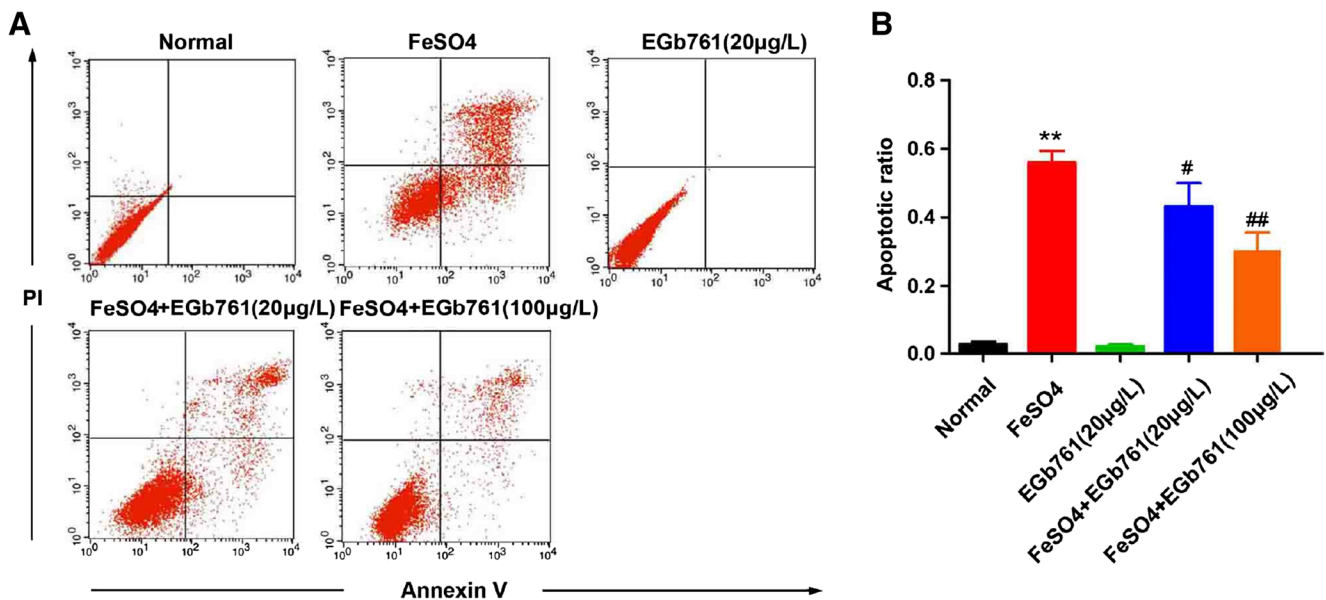


Fig. 3 Effect of EGb761 on ferrous iron-induced apoptosis in primary cultured cortical neurons. Cell apoptosis were detected by flow cytometry using Annexin V-FITC and propidium iodide (PI) (a). Flow cytometric

analysis (b) showed that EGb761 significantly attenuated neuronal apoptosis induced by ferrous iron (** $p < 0.01$, as compared with normal control; # $p < 0.05$, ## $p < 0.01$, as compared with FeSO₄)

be associated with self-protective response in the brain. It was even higher in the EGb761 group, indicating that EGb761 downregulation of GSK3 β activity was mediated via phosphorylation GSK3 β at Ser9. A higher level of pGSK3 β (Tyr216) expression was also observed in ICH, vehicle, and EGb761, compared with the sham group. However, EGb761 was unable to influence its expression further compared with the ICH and vehicle groups. RSK1 is one of the GSK3 β upstream proteins. The role of RSK1 in the pathophysiological mechanism of ICH is unknown. Although RSK1 expression after ICH was no different from that of the sham group, it was significantly increased after administration of EGb761. Temporal differences in pGSK3 β (Ser9) between the vehicle and EGb761 groups are shown in Fig. 4C. On day 1, the pGSK3 β (Ser9) level was not affected by EGb761 significantly, and from day 3 to day 21, EGb761 increased GSK3 β (Ser9) expression compared with vehicle treatment. RSK1 shRNA treatment significantly decreased the level of RSK1 and repressed the phosphorylation of GSK3 β (Ser9) by EGb761 (Fig. 5).

The nuclear levels of pGSK3 β (Ser9) play an important role in apoptosis [15, 40]. We determined the expression of pGSK3 β (Ser9) in the nuclear and cytoplasmic fractions, respectively, using Western blot (Fig. 6A). We found that both the nuclear and cytoplasmic levels of the protein were dramatically higher in the EGb761 group than in the vehicle group. Immunofluorescence staining was also used to examine subcellular distributions of pGSK3 β (Ser9). As illustrated in Fig. 6B, the nuclear accumulation of pGSK3 β (Ser9) was more frequently observed in the EGb761 group.

Apoptosis-related proteins Bcl2, Bax, and CC3 were also examined. The ratio of Bcl2 to Bax was significantly increased in the EGb761-treated mice and CC3 was repressed compared with the vehicle-treated mice (Fig. 6C).

In vitro, ferrous iron exposure markedly decreased pGSK3 β (Ser9), which was reversed by treatment with EGb761 prior to ferrous iron exposure. A significant increase in the Bcl2-to-Bax ratio and decrease in CC3 occurred. No difference in the expression of pGSK3 β (Tyr216) was found in any group suggesting that ferrous iron exposure downregulated the expression of pGSK3 β (Ser9) and induced neuronal apoptosis, which was ameliorated by EGb761 (Fig. 7).

Discussion

In this study, we demonstrated that EGb761 treatment reduced the neurological deficits in a mouse model of ICH and inhibited apoptosis in neurons. The possible mechanisms include increased expression of RSK1 following EGb761 treatment, which promoted inhibition of GSK3 β via phosphorylation at serine-9. Our results also suggested that EGb761 improved angiogenesis after ICH by upregulating the expression of VEGF.

Our findings suggested that downregulation of GSK3 β activity is a promising neuroprotective mechanism and EGb761 suppressed GSK3 β activity. In our animal study, both Ser9 and Tyr216 phosphorylation of GSK3 β were significantly elevated after ICH and the activity of GSK3 β was increased in ICH compared with the sham group. Interestingly, our in vitro results showed that ferrous iron

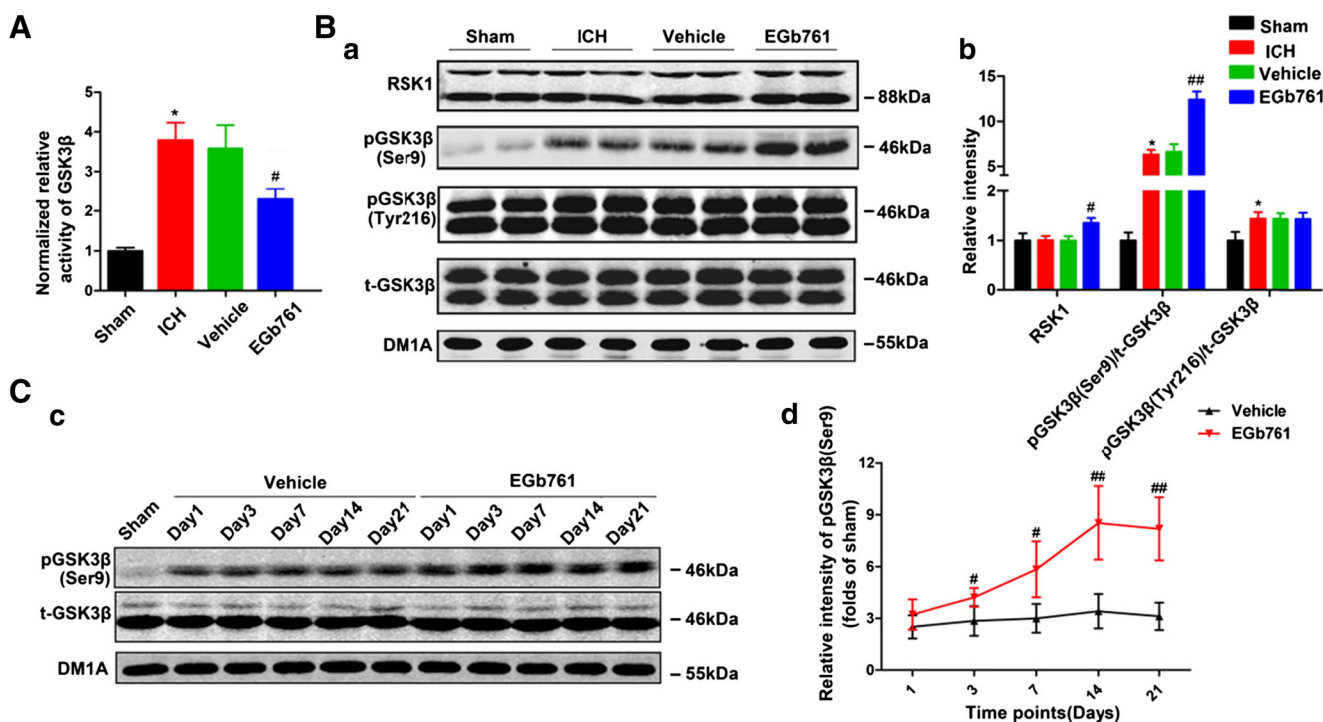


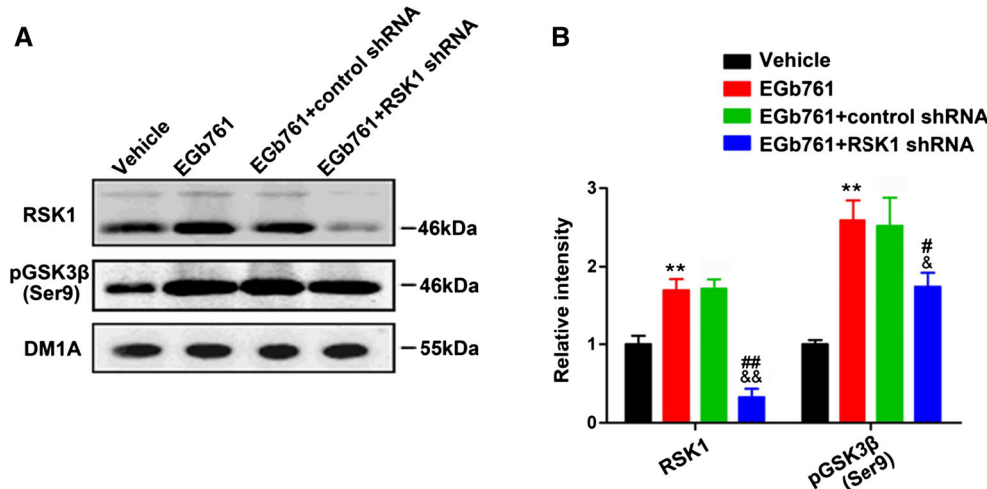
Fig. 4 Mice brain GSK3 β kinase activities were detected at day 7 (**A**). We found that the activity of GSK3 β was increased markedly in response to ICH ($n = 4$, each group; $*p < 0.05$, as compared with the sham group; $#p < 0.05$, as compared with the vehicle group). As the activity of GSK3 β was modulated by phosphorylation at Ser9 (inactive) and Tyr216 (active), we therefore determined these two phosphorylation sites using Western blot. As shown in **B**, the pGSK3 β (Ser9) level was higher in the ICH and vehicle group compared with that in the sham group and whereas it was even higher in the EGb761 group ($n = 4$, each group; $*p < 0.05$, as compared with the sham group; $##p < 0.01$, as compared with the vehicle group). A higher level of pGSK3 β (Tyr216) expression was also observed in the ICH, vehicle, and EGb761 groups, when compared

with that in the sham group ($n = 4$, each group; $*p < 0.05$, as compared with the sham group). However, EGb761 was not able to influence its expression, compared with the ICH and vehicle groups. In **B**, although RSK1 expression level in the ICH and vehicle groups has no difference between the sham group, it was significantly increased after administration of EGb761 ($n = 4$, each group; $#p < 0.05$, as compared with the vehicle group). Temporal differences of pGSK3 β (Ser9) between the vehicle and EGb761 groups are shown in **C**. On day 1, the pGSK3 β (Ser9) level was not affected by EGb761 significantly and from day 3 to day 21, EGb761 increased the GSK3 β (Ser9) expression compared with the vehicle treatment ($n = 4$, each group; $*p < 0.05$, $##p < 0.01$, as compared with the vehicle group)

increased neuronal apoptosis and decreased the phospho-GSK3 β (Ser9), while the levels of phospho-GSK3 β (Tyr216) remained constant. The discrepancies between the in vitro and in vivo findings may be related to GSK3 β

response in other cells of the central nervous system in addition to neurons. Therefore, it was probably that in response to ICH, GSK3 β Ser9 phosphorylation increased in the brain, which was probably attributed to an adaptive self-protection

Fig. 5 RSK1 shRNA treatment significantly decreased the level of RSK1 and repressed the induction of phosphorylation GSK3 β (Ser9) by EGb761 (**a, b**) ($p < 0.05$) ($n = 4$, each group; $**p < 0.01$, as compared with the vehicle group; $#p < 0.05$, $##p < 0.01$, as compared with the EGb761 + control shRNA group; $&p < 0.05$, $&&p < 0.01$, as compared with the EGb761 group)



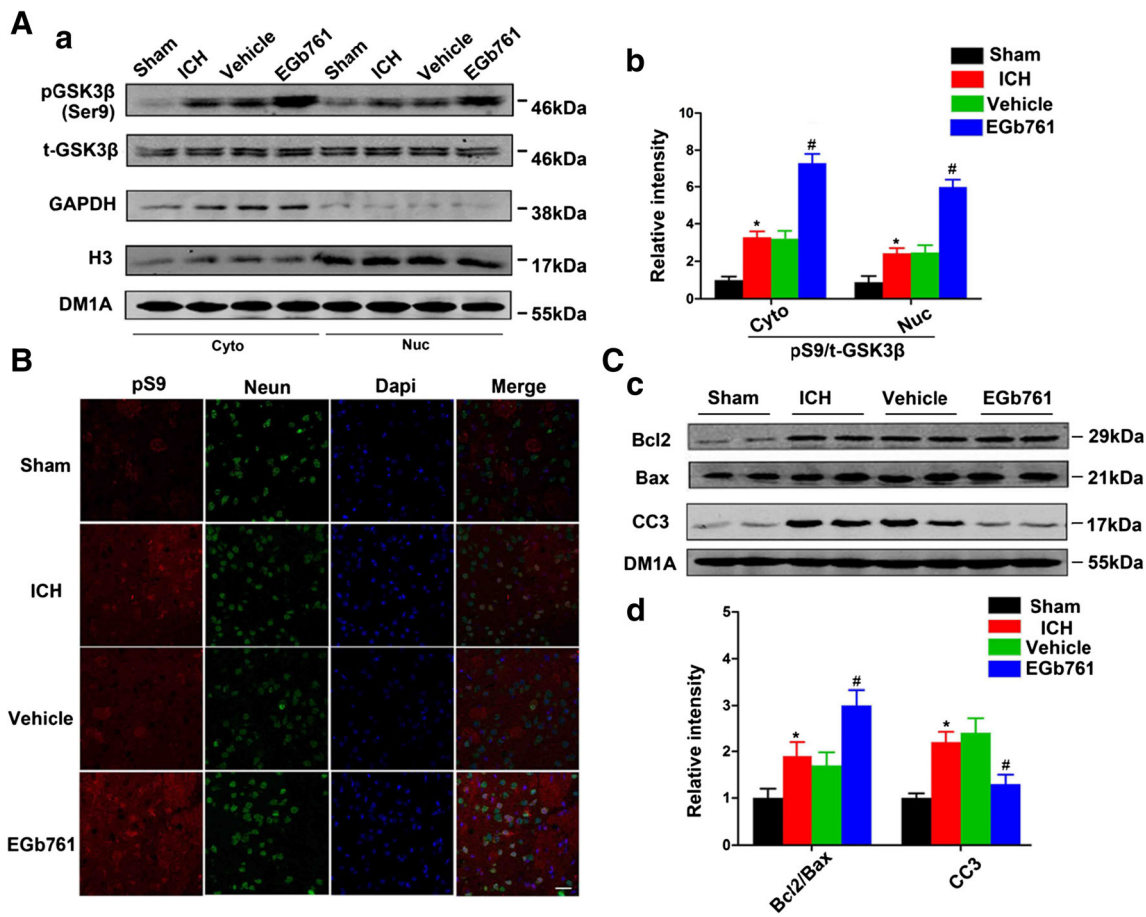


Fig. 6 The level of pGSK3 β (Ser9) in nuclei is more relevant with apoptosis process. Nuclear and cytoplasmic fractions were extracted for Western blot. No matter in nucleus and cytoplasm, the relative level of Ser-9-phosphorylated GSK3 β in the EGb761 group was higher than in the vehicle group (A) ($n = 4$, each group; $*p < 0.05$, vs. as compared with the sham group; $#p < 0.05$, vs. as compared with the vehicle group). Immunofluorescence staining was also used to examine subcellular

distributions of pGSK3 β (Ser9). As illustrated in B, the accumulation of pGSK3 β (Ser9) in the nucleus was more commonly seen in the EGb761 group ($n = 6$, each group; scale bar = 20 μm). Western blot showed that EGb761 significantly increased the expression of Bcl2 to Bax ratio and decreased the apoptotic-related cleaved-caspase 3 (CC3) (C) ($n = 4$, each group; $*p < 0.05$, as compared with the sham group; $#p < 0.05$, as compared with the vehicle group)

mechanism. The Tyr216 phosphorylation was increased concomitantly during the pathophysiology of ICH. Our data also demonstrated a possible neuroprotective mechanism involving EGb761-mediated selective upregulation of GSK3 β phosphorylation at Ser9 independent of Tyr216 phosphorylation both in vivo and in vitro, resulting in decreased GSK3 β activity and cellular apoptosis.

The altered expression of RSK1 and the relationship between RSK1 and GSK3 β after ICH was not reported previously. Using Western blot, we initially found no difference in the expression of RSK1 between the sham and ICH groups, indicating that RSK1 may not mediate the posthemorrhagic pathophysiology or autorepair mechanisms. Nevertheless, the EGb761-induced overexpression of endogenous RSK1 was sufficient to inhibit GSK3 β activity via serine-9 phosphorylation. Moreover, administration of RSK1 shRNA dramatically inhibited RSK1 levels in the EGb761 group, leading to neutralization of EGb761-mediated pGSK3 β (ser9) upregulation,

indicating that EGb761 increased pGSK3 β (ser9) level through upregulation of RSK1. The RSK1/GSK3 β signal transduction pathway may be a promising and potential therapeutic target in ICH.

Angiogenesis is essential to neurological recovery, which is regulated by several angiogenic factors, such as VEGF [15, 40–42]. ICH-induced angiogenesis generally occurs along the border of the hematoma in 7 days after hemorrhage, gradually extending into the center of hematoma. New blood vessels appear scattered all over the blood clot in about 21 days [40]. Therefore, we used MOST to determine the vascular networks in mice 21 days after ICH to ensure relatively complete observation of angiogenesis after ICH. We initially used modified Nissl staining combined with MOST to directly visualize the deep brain neurovascular structures in diseased mouse brains. MOST provides a maximum resolution of 0.33 μm to reveal the cellular and vascular configuration and observe individual vessel and neuronal morphology

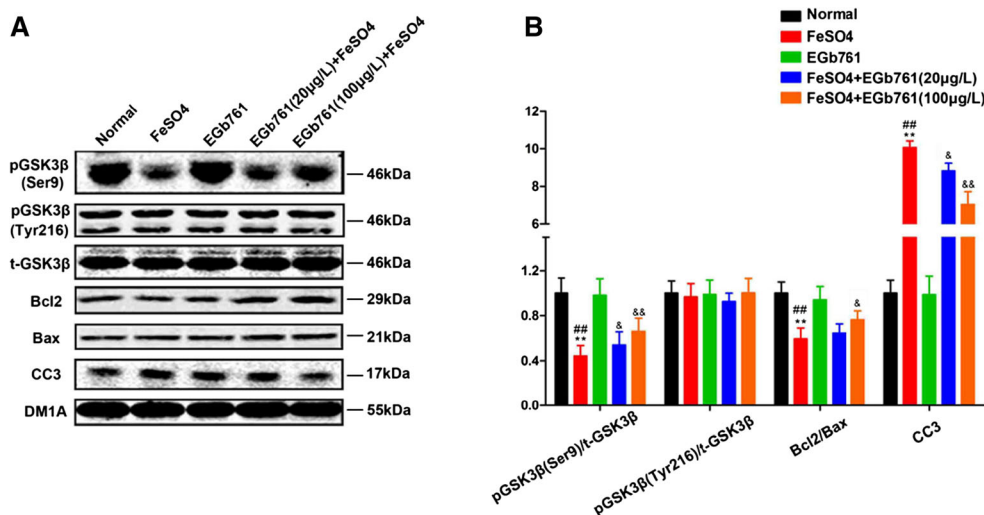


Fig. 7 The expression of pGSK3 β (Ser9), pGSK3 β (Tyr216), GSK3 β , Bcl2, Bax, and cleaved-caspase3 (CC3) in primary cultured neurons were assessed by Western blot (a). Ferrous iron (FeSO $_4$) decreased the expression of pGSK3 β (Ser9). EGb761 reversed the downregulation of pGSK3 β (Ser9) expression induced by ferrous iron. On the other hand,

the expression of pGSK3 β (Tyr216) had no difference among all groups. EGb761 significantly increased the expression of Bcl2 to Bax ratio and decreased the CC3 expression (b) (** $p < 0.01$, as compared with the normal control; # $p < 0.05$, ## $p < 0.01$, as compared with the EGb761 group; & $p < 0.05$, && $p < 0.01$, as compared with the FeSO $_4$ group)

[32]. In this study, the microvessel density of the lesions was significantly higher in the EGb761-treated mice compared with that of the vehicle group. We also compared the normal microvessels contralateral to the lesions in the EGb761 group with the vehicle group. The similar phenomenon was observed after treatment with EGb761 for 21 consecutive days. The density of the microvessel plexus was also increased. We speculated that the EGb761-induced VEGF increase, observed by Western blot, was probably the underlying mechanism.

It is well known that cerebrovascular rupture releases a large number of blood cells into brain parenchyma. Subsequently, the blood-brain barrier is severely disrupted followed by inflammatory cell infiltration. Neuronal cells in the hemorrhagic side are fewer than in the normal side due to neuronal apoptosis. In addition, the death and degeneration of hematocytes and inflammatory cells are observed. Cell debris and degradation products may be non-specifically stained by Nissl dye. These changes may explain the increase in cell number counted in 3D images of the lesion side compared with the unaffected normal side. Based on the initial application of MOST, which is a newly developed imaging modality in diseased mouse brains, we considered a possible role in neurodegenerative, neurogenetic, and metabolic diseases of the nervous system such as AD, PD, and depression, more than in traumatic brain injury or brain infarction. In the future, projects involving whole-brain research, such as ICH, may include determination of 3D spatial architecture of neurovascular units, neuronal projection tracing, and synaptic connections.

The study limitations were as follows. First, until now, four phosphorylation sites (Ser221, Ser363, Ser380, and Thr573)

were found to affect the activity of RSK1 [17]. In this study, we initially observed that the expression of RSK1 was enhanced after EGb761 treatment. Nevertheless, the phosphorylated isoforms of activated RSK1 following EGb761 treatment were not studied. Second, we identified microvessels in the EGb761 group more intensely via MOST. However, we were unable to validate the functionality of the microvessels observed and improvement in cerebral perfusion, which needs further investigation.

In conclusion, our findings suggested that EGb761 improved the functional outcome and attenuated neuronal apoptosis via the RSK1/GSK3 β pathway. EGb761 promoted angiogenesis by increasing VEGF expression after ICH.

Acknowledgements This investigation was supported by Prof. Zhouping Tang's National Natural Science Foundation of China (81171089, 81471211). We would like to express our gratitude to Dr. Teng Zhang for his assistance in this experiment.

We are very grateful to Wuhan Oebio Biology Co., Ltd. (<http://www.oebio.com/>) for kindly assisting us with the MOST technique used in the reconstruction of 3D neurovascular networks. *Ginkgo biloba* (EGb761) was kindly provided by Dr. Willmar Schwabe Pharmaceuticals, Germany.

Authors' Contributions Chao Pan performed most of the experiments and drafted the manuscript; Na Liu and Ping Zhang conducted the neuronal culture studies; Qian Wu performed the flow cytometry; Hong Deng established the animal models; Feng Xu bred the mice and conducted the behavioral tests; Lifei Lian and Qiming Liang performed the Western blot; Yang Hu conducted the statistical analysis; and Prof. Zhouping Tang and Suiqiang Zhu designed and guided the experiments.

Compliance with Ethical Standards

Conflict of Interest The authors declare that they have no competing interests.

Glossary

AD	Alzheimer's disease
CC3	Cleaved-caspase3
GSK3 β	Glycogen synthase kinase-3 β
ICH	Intracerebral hemorrhage
mNSS	Modified neurological severity score
MOST	Micro-optical sectioning tomography
PD	Parkinson's disease
pGSK3 β	Phosphorylated-GSK3 β
PI	Propidium iodide
RNAi	RNA interference
RSK1	p90 ribosomal S6 kinase 1
SAH	Subarachnoid hemorrhage

References

- Qureshi AI, Mendelow AD, Hanley DF (2009) Intracerebral haemorrhage. *Lancet* 373(9675):1632–1644
- Wilson D, Adams ME, Robertson F, Murphy M, Werring DJ (2015) Investigating intracerebral haemorrhage. *BMJ* 350:h2484
- Qureshi AI, Tuhim S, Broderick JP, Batjer HH, Hondo H, Hanley DF (2001) Spontaneous intracerebral hemorrhage. *N Engl J Med* 344(19):1450–1460
- Labovitz DL, Halim A, Boden-Albala B, Hauser WA, Sacco RL (2005) The incidence of deep and lobar intracerebral hemorrhage in whites, blacks, and hispanics. *Neurology* 65(4):518–522
- Sudlow CL, Warlow CP (1997) Comparable studies of the incidence of stroke and its pathological types: results from an international collaboration. *Stroke* 28(3):491–499
- Mikulik R, Wahlgren N (2015) Treatment of acute stroke: an update. *J Intern Med* 278(2):145–165
- Gong C, Boulis N, Qian J, Turner DE, Hoff JT, Keep RF (2001) Intracerebral hemorrhage-induced neuronal death. *Neurosurgery* 48(4):875–882
- Mracsko E, Veltkamp R (2014) Neuroinflammation after intracerebral hemorrhage. *Front Cell Neurosci* 8:388
- Xi G, Keep RF, Hoff JT (2006) Mechanisms of brain injury after intracerebral haemorrhage. *Lancet Neurol* 5(1):53–63
- Takahashi-Yanaga F (2013) Activator or inhibitor? GSK-3 as a new drug target. *Biochem Pharmacol* 86(2):191–199
- Chiara F, Rasola A (2013) GSK-3 and mitochondria in cancer cells. *Front Oncol* 3:16
- Kaidanovich-Beilin O, Woodgett JR (2011) GSK-3: functional insights from cell biology and animal models. *Front Mol Neurosci* 4:40
- Vossel KA, Xu JC, Fomenko V, Miyamoto T, Suberbielle E, Knox JA, Ho K, Kim DH et al (2015) Tau reduction prevents A β -induced axonal transport deficits by blocking activation of GSK-3 β . *J Cell Biol* 209(3):419–433
- Miyawaki T, Ofengeim D, Noh KM, Latuszek-Barrantes A, Hemmings BA, Follenzi A, Zukin RS (2009) The endogenous inhibitor of Akt, CTMP, is critical to ischemia-induced neuronal death. *Nat Neurosci* 12(5):618–626
- Lee HC, Lin YZ, Lai YT, Huang WJ, Hu JR, Tsai JN, Tsai HJ (2014) Glycogen synthase kinase 3 beta in somites plays a role during the angiogenesis of zebrafish embryos. *FEBS J* 281(19):4367–4383
- Romeo Y, Zhang X, Roux PP (2012) Regulation and function of the RSK family of protein kinases. *Biochem J* 441(2):553–569
- Frodin M, Gammeltoft S (1999) Role and regulation of 90 kDa ribosomal s6 kinase (RSK) in signal transduction. *Mol Cell Endocrinol* 151(1–2):65–77
- Stambolic V, Woodgett JR (1994) Mitogen inactivation of glycogen synthase kinase-3 beta in intact cells via serine 9 phosphorylation. *Biochem J* 303(Pt 3):701–704
- Diamond BJ, Bailey MR (2013) *Ginkgo biloba*: indications, mechanisms, and safety. *Psychiatr Clin North Am* 36(1):73–83
- Janssen IM, Sturtz S, Skipka G, Zentner A, Velasco GM, Busse R (2010) *Ginkgo biloba* in Alzheimer's disease: a systematic review. *Wien Med Wochenschr* 160(21–22):539–546
- Weinmann S, Roll S, Schwarzbach C, Vauth C, Willich SN (2010) Effects of *Ginkgo biloba* in dementia: systematic review and meta-analysis. *BMC Geriatr* 10:14
- Sun BL, Yuan H, Yang MF, Xia ZL, Zhang SM, Wang LX (2007) Effects of extract of *Ginkgo biloba* on intracranial pressure, cerebral perfusion pressure, and cerebral blood flow in a rat model of subarachnoid haemorrhage. *Int J Neurosci* 117(5):655–665
- Tanaka K, Galduroz RF, Gobbi LT, Galduroz JC (2013) *Ginkgo biloba* extract in an animal model of Parkinson's disease: a systematic review. *Curr Neuropharmacol* 11(4):430–435
- Yan M, Liu YW, Shao W, Mao XG, Yang M, Ye ZX, Liang W, Luo ZJ (2016) EGb761 improves histological and functional recovery in rats with acute spinal cord contusion injury. *Spinal Cord* 54(4):259–265
- Sun L, Zhuang W, Xu X, Yang J, Teng J, Zhang F (2013) The effect of injection of EGb761 into the lateral ventricle on hippocampal cell apoptosis and stem cell stimulation in situ of the ischemic/reperfusion rat model. *Neurosci Lett* 555:123–128
- Kwon KJ, Lee EJ, Cho KS, Cho DH, Shin CY, Han SH (2015) *Ginkgo biloba* extract (EGb761) attenuates zinc-induced tau phosphorylation at ser262 by regulating gsk3beta activity in rat primary cortical neurons. *Food Funct* 6(6):2058–2067
- Sun BL, Hu DM, Yuan H, Ye WJ, Wang XC, Xia ZL, Zhang SM, Wang LX (2009) Extract of *Ginkgo biloba* promotes the expression of VEGF following subarachnoid hemorrhage in rats. *Int J Neurosci* 119(7):995–1005
- Nada SE, Tulsulkar J, Shah ZA (2014) Heme oxygenase 1-mediated neurogenesis is enhanced by *Ginkgo biloba* (EGb 761®) after permanent ischemic stroke in mice. *Mol Neurobiol* 49(2):945–956
- Gao X, Lin B, Sadayappan S, Patel TB (2014) Interactions between the regulatory subunit of type I protein kinase a and p90 ribosomal S6 Kinase1 regulate cardiomyocyte apoptosis. *Mol Pharmacol* 85(2):357–367
- Chen J, Tang YX, Liu YM, Chen J, Hu XQ, Liu N, Wang SX, Zhang Y et al (2012) Transplantation of adipose-derived stem cells is associated with neural differentiation and functional improvement in a rat model of intracerebral hemorrhage. *CNS Neurosci Ther* 18(10):847–854
- Chen J, Li Y, Wang L, Zhang Z, Lu D, Lu M, Chopp M (2001) Therapeutic benefit of intravenous administration of bone marrow stromal cells after cerebral ischemia in rats. *Stroke* 32(4):1005–1011
- Li A, Gong H, Zhang B, Wang Q, Yan C, Wu J, Liu Q, Zeng S et al (2010) Micro-optical sectioning tomography to obtain a high-resolution atlas of the mouse brain. *Science* 330(6009):1404–1408
- Wu J, He Y, Yang Z, Guo C, Luo Q, Zhou W, Chen S, Li A et al (2014) 3D brain CV: simultaneous visualization and analysis of cells and capillaries in a whole mouse brain with one-micron voxel resolution. *NeuroImage* 87:199–208
- Pei L, Shang Y, Jin H, Wang S, Wei N, Yan H, Wu Y, Yao C et al (2014) DAPK1-p53 interaction converges necrotic and apoptotic pathways of ischemic neuronal death. *J Neurosci* 34(19):6546–6556

35. Liu D, Wei N, Man HY, Lu Y, Zhu LQ, Wang JZ (2015) The MT2 receptor stimulates axonogenesis and enhances synaptic transmission by activating Akt signaling. *Cell Death Differ* 22(4):583–596
36. Chen J, Regan RF (2004) Heme oxygenase-2 gene deletion increases astrocyte vulnerability to hemin. *Biochem Biophys Res Commun* 318(1):88–94
37. Chen-Roetling J, Chen L, Regan RF (2009) Minocycline attenuates iron neurotoxicity in cortical cell cultures. *Biochem Biophys Res Commun* 386(2):322–326
38. Pei L, Wang S, Jin H, Bi L, Wei N, Yan H, Yang X, Yao C et al (2015) A novel mechanism of spine damages in stroke via DAPK1 and tau. *Cereb Cortex* 25(11):4559–4571
39. Qu N, Zhou XY, Han L, Wang L, Xu JX, Zhang T, Jiang C, Qiao C et al (2016) Combination of PPT with LiCl treatment prevented bilateral ovariectomy-induced hippocampal-dependent cognition deficit in rats. *Mol Neurobiol* 53(2):894–904
40. Tang T, Liu XJ, Zhang ZQ, Zhou HJ, Luo JK, Huang JF, Yang QD, Li XQ (2007) Cerebral angiogenesis after collagenase-induced intracerebral hemorrhage in rats. *Brain Res* 1175:134–142
41. Arai K, Jin G, Navaratna D, Lo EH (2009) Brain angiogenesis in developmental and pathological processes: neurovascular injury and angiogenic recovery after stroke. *FEBS J* 276(17):4644–4652
42. Seto SW, Chang D, Jenkins A, Bensoussan A, Kiat H (2016) Angiogenesis in ischemic stroke and angiogenic effects of Chinese herbal medicine. *J Clin Med* 5(6). doi:10.3390/jcm5060056